Molecular Science

AIMS Molecular Science, 4 (3):352-369.
DOI: 10.3934/molsci.2017.3.352
Received 13 July 2017,
Accepted 17 September 2017,
Published 22 September 2017

http://www.aimspress.com/journal/Molecular

Research article

Simulation of lipid-protein interactions with the CgProt force field

Jacob Fosso-Tande[1], Cody Black[1], Stephen G. Aller[2], Lanyuan Lu[3], and Ronald D. Hills Jr[1,*]

[1] Department of Pharmaceutical Sciences, College of Pharmacy, University of New England, Portland, Maine, USA

[2] Department of Pharmacology and Toxicology, University of Alabama at Birmingham, Birmingham, Alabama, USA

[3] School of Biological Sciences, Nanyang Technological University, Nanyang, Singapore

* **Correspondence:** Email: rhills@une.edu; Tel: (207) 221-4049.

Abstract: The effect of lipid-protein interactions on membrane proteins and their function is emerging as an important area in biophysics. The recently developed CgProt force field is used to explore molecular level interactions in peptides and proteins through coarse-grained molecular dynamics simulations in the presence of the lipid bilayer environment. The mechanism of membrane insertion was examined for designed helical peptides WALP27: GWW$(LA)_{10}$LWWA and LS3: $(LSSLLSL)_3$. WALP27 adopts a transmembrane conformation while LS3 adopts interfacial and transmembrane orientations in independent simulations from different starting conditions. A total of 13 peptide insertion events were observed in unbiased molecular dynamics simulations of LS3 and WALP. Each case proceeded via the charged N-terminus crossing the bilayer. In the equilibrated conformations, the C-terminus resides in the head group region of the DOPC bilayer, while the N-terminus submerges deep into the carbonyl region. These findings are consistent with recent evidence of the attractive nature of positive charges for the membrane interface. The role of lipid interactions in the native environment of a membrane protein was explored by simulation of a 12-transmembrane helix multidrug transporter, P-glycoprotein. Analysis of the lipid density in a POPC: POPE bilayer containing 20% cholesterol revealed an annular solvation shell of phosphatidyl choline and cholesterol that diffuses with the protein in the membrane. The inward-facing state of P-glycoprotein undergoes a conformational transition to the closed state, corroborating a structural model for the ATP-bound state recently generated by homology modeling and molecular dynamics simulation.

Keywords: molecular dynamics simulation; multiscale modeling; membrane proteins; ABC transporters; lipid-protein interactions

Abbreviations

CG: coarse-grained
L24: $KKL_{24}KK$ peptide
LS3: $(LSSLLSL)_3$ interfacial helix
MD: molecular dynamics
MS-CG: multiscale coarse graining
NBD: nucleotide-binding domain
P-gp: p-glycoprotein
PMF: potential of mean force
POPC: palmitoyl-oleoyl phosphatidyl choline
POPE: palmitoyl-oleoyl phosphatidyl ethanolamine
RMSD: root-mean-square deviation
TM: transmembrane
WALP27: $GWW(LA)_{10}LWWA$ transmembrane peptide

1. Introduction

Elucidating the interactions of proteins with their native membrane environment is central to our understanding of the function of cell membrane proteins and receptors [1,2]. Atomistic force fields enable detailed simulations of membrane dynamics [3-6], but the lateral diffusion of lipids in the bilayer is slow to converge and requires large system sizes [7]. Coarse-grained (CG) model representations group atoms into effective interaction centers to strike a balance between chemical detail and computational efficiency, expanding the range of problems that can be explored [8]. Coarse graining lipid bilayers has become a powerful tool for studying the dynamics of complex multicomponent membrane systems [9]. CG models of polypeptides, initially developed to study protein folding [10], can now be applied to conformational transitions and protein functional mechanisms [11-14]. To understand how the local membrane environment modulates protein function, care must be taken to incorporate a protein's conformational flexibility in the context of the lipid bilayer environment [15-20]. CG simulations have identified direct and indirect effects on protein function arising from the presence of cholesterol as well as anionic [21-23], zwitterionic and double phospholipids in the bilayer [20,24,25].

MARTINI is a widely-used CG force field rooted in a thermodynamics-based parameterization approach [26]. The resulting protein and lipid models have been characterized rather extensively and parameter sets are now available for dozens of membrane lipid types [27-36]. While simulations with the model have yielded numerous insights into multicomponent systems of biological interest [9,13,34,37], there are limitations inherent in the model [29,38]. The nonbond interaction potentials rely on the Lennard-Jones 12-6 functional form, which for CG representations has been shown to have a core repulsion that is steeper than the corresponding atomistic molecular dynamics (MD) distributions [39,40]. Another potential issue is that MARTINI solvent particles, each of which represents four water molecules, have a tendency to freeze at room temperature [38].

Explorations of protein conformational dynamics will be limited if the CG pseudodihedral potential energy function fixes the secondary structure assigned in the starting conformation [37]. Flexible bonded and nonbonded potentials are useful in protein folding studies but structural collapse is a potential problem when implementing them in CG force fields not intended for folding [40,41]. Other ongoing developments in the field include incorporating polarizable CG water beads that are

still consistent with the protein parameters and capture the context dependence of interactions [41,42-45]. Martini version 2.2P incorporates polarized polar sidechains in order to obtain the expected attractive behavior at the membrane interface [46]. Dry Martini avoids the issues associated with large CG solvent particles by removing the explicit waters but retaining all bilayer lipids [33,47,48]. To better balance the treatment of protein versus solvent water interactions, Han et al. developed the PACE united-atom protein force field for simulations in the presence of CG water [49,50]. Unlike the Cα-only model employed for the backbone in many CG models, incorporating explicit backbone amide atoms is ideal for studies of protein folding that depend on backbone hydrogen bonding. A promising new CG approach that allows for secondary structure formation is to introduce a polarizable dipole into a Cα-only backbone bead [51].

The present work explores the utility of the CgProt force field for simulations of peptides and proteins in an explicit bilayer. As opposed to parameterizing particles individually using thermodynamic solvation data, CgProt is rooted in the multiscale coarse graining (MS-CG) method [40,52]. MS-CG takes a large set of reference configurations in one or more atomistic MD simulations and uses a variational force-matching scheme to simultaneously develop a self-consistent set of CG interaction potentials. Tabulated potentials can be constructed for the nonbond interactions with no a priori assumptions of their functional form [53]. Nonbond tables with 0.005 nm or smaller bins can then be read in by the Gromacs simulation package for efficient CG-MD simulations [54]. A technical limitation is that GPU-acceleration is not yet supported (as of Gromacs 2016.3), because the group cutoff scheme is needed for tabulated potentials. To avoid the pitfalls associated with bulky CG water particles, the water degrees of freedom are integrated out with their effects on solvation captured implicitly in the nonbond potentials [47]. Note that because of the additive nature of many-body interactions, each pairwise MS-CG potential in the set is not equivalent to a potential of mean force (PMF) calculation obtained from on an individual particle pair [53].

The CgProt protein model is derived from folding simulations in water [40], while the lipid-protein interactions were developed from MS-CG calculations on unfolded peptide-phospholipid ensembles [20]. The lipid parameter set was recently improved upon to include lipids abundant in eukaryotic and prokaryotic membranes: POPC, POPE, POPG, cardiolipin and cholesterol [55]. To obtain better agreement with atomistic simulations, a more repulsive potential was incorporated for phosphatidyl ethanolamine (PE) head groups, along with a harmonic torsion to capture the configurational influence of a cis double bond on the acyl chain.

In the present work, the mechanism of insertion was examined for peptide helixes WALP27, LS3 and L24 in a DOPC bilayer. Multiple, independent unbiased CgProt simulations were performed starting from either inserted or desorbed peptide conformational states. Next, CgProt was used to demonstrate the conformational transition of the 1,188-residue, 12-transmembrane helix ABC transporter P-glycoprotein (P-gp). The conformational change involved a hinge bending motion and reorientation between the protein's two pseudosymmetric halves and did not require changes in secondary structure. To examine the potential role of lipid-protein interactions, molecular dynamics were performed in a 17 nm patch of model eukaryotic membrane containing a symmetric 2:2:1 ratio of POPC: POPE: cholesterol.

2. Materials and Methods

In CgProt 2.3 the polypeptide is represented as a Cα chain with up to 4 interaction sites defined for each sidechain (Figure 1). To match fluctuations observed in atomistic MD, harmonic Cα-Cα

bonds are assigned an effective force constant of 80,000 kJ mol^{-1} nm^{-2} with 3.86 Å equilibrium length. By comparison, variants of the Martini model limit all bond constants to a maximum of 7500 kJ mol^{-1} nm^{-2} to allow for a larger integration time step [11,56-58]. CgProt employs double-well bonded potentials for 3-body backbone Cα angles and 4-body pseudotorsions that allow for both α-helix and β-sheet secondary structure [11,40,59]. To maintain amino acid chirality [60,61], an improper torsion term is applied to residues with a Cβ site in the sidechain [11]. All 1,2 and 1,3 bonded interaction pairs are excluded from nonbonded interactions, as are 1,4 backbone Cα pairs. Flexible angle terms for CG sidechain sites were developed as 4th order polynomials via Boltzmann inversion of flexible peptide simulations [40]. Only the Trp and Tyr sidechains have dihedral terms to maintain ring planarity. Harmonic sidechain pseudobond potentials are representative of their corresponding atomistic fluctuations in solution with a maximum force constant of 100,000 kJ mol^{-1} nm^{-2} to allow for up to an 8 fs integration time step [11]. The liquid bilayer phase is maintained at kT = 2.24 kJ/mol in Gromacs 4.6.7 using stochastic Langevin dynamics with a damping friction coefficient of $\gamma = 0.5$ ps^{-1} [54,55]. The neighbor list is updated every step for the tabulated nonbond potentials (1.2 nm cutoff distances), which combine van der Waals and electrostatic contributions into a single PMF. As $\gamma = 50$ ps^{-1} in real water [62], the CG bilayer and implicit solvent represent a significant computational speedup. Lipids in CgProt exhibit lateral diffusion coefficients ≥ 250 μm^2 s^{-1}, a 30-fold enhancement relative to experimental values for the liquid bilayer phase [7,20].

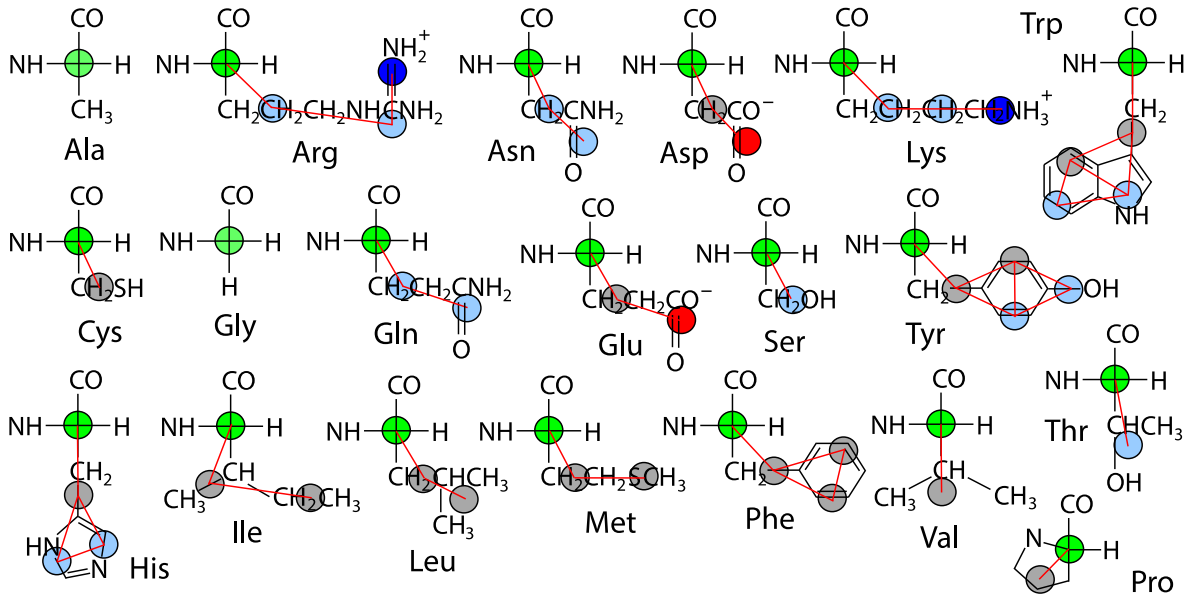

Figure 1. Site assignments for backbone (green) and sidechains (assorted colors). Functional groups are represented by apolar (gray), polar (cyan), positive (blue) and negative (red) site types. Pseudobonds are represented by red lines. The model assigns one more interaction center than the widely used MARTINI force field for sidechains Arg/Lys, Asn/Gln, Asp/Glu, Ile/Leu/Met and Tyr.

2.1. Peptide insertion simulations

The mechanism of membrane binding and insertion of synthetic peptides is explored in a DOPC bilayer [30,31,63-66]. The sequence $GWW(LA)_{10}LWWA$ (WALP27) of the WALP *n* series of single-pass transmembrane peptides was simulated since its 31.5 Å hydrophobic length is the closest

match for the hydrophobic thickness of the DOPC bilayer: 29 Å as measured by the mean distance between acyl ester groups [67]. The highly charged transmembrane peptide $K_2L_{24}K_2$ (L24) was also assessed for its bilayer insertion stability [68]. Third, the designed amphipathic peptide $(LSSLLSL)_3$, referred to as LS3, was assessed for its binding behavior at the membrane-water interface [69]. Peptide N- and C-terminal alpha carbons were assigned the default positive and negative site types, respectively, as there is no Coulomb potential in CgProt.

While previous simulations relied an elastic network model of native contacts to stabilize the backbone in tertiary protein domains [20], distance restraints were not sufficient to stabilize a single ideal α-helix. In the case of LS3, polar residues did not remain aligned on the same side of the helix. Backbone alpha carbons were therefore restrained using GROMOS-96 angles (θ_0 = 89°, k_θ = 2000 kJ mol^{-1}) and harmonic dihedrals (φ_0 = 50°, k_φ = 2000 kJ mol^{-1} rad^{-2}) in all three peptides. For MD analysis, translational motion of the bilayer center of mass in the z-dimension was removed from each trajectory by root-mean-square alignment of the ester sites with the starting configuration. The angle of the peptide insertion with respect to the bilayer normal was calculated using the vector spanning alpha carbons 5 and 16 for LS3, 6 and 24 for WALP27, and 8 and 26 for L24. Peptides were simulated in multiple independent 500 ns simulation runs with 1,148 DOPC molecules in a 20 nm square box, each requiring 80 hours on 48 CPUs.

2.2. P-gp membrane simulation

The refined crystal structure (PDB ID: 4M1M) for mouse P-gp was simulated to investigate the conformational dynamics of the ABC transporter in a eukaryotic model membrane [70]. The missing flexible linker in the structure between its N- and C-terminal halves was omitted; these two terminal residues employed the Cα nonbond site type (uncharged). The seven cis peptide bonds in P-gp were assigned a 3.1 Å harmonic Cα-Cα bond. While complex algorithms have been developed for inserting protein structures into a lipid bilayer [71], the following procedure was used to expedite creating a pore around the protein. System preparation began with deleting the L24 peptide coordinates from a 17.1 nm square bilayer patch previously equilibrated with 472 palmitoyl-oleoyl phosphatidyl choline (POPC), 446 palmitoyl-oleoyl phosphatidyl ethanolamine (POPE), and 230 cholesterol lipids (50.7 Å area/lipid). A 1 ns simulation was performed with applied surface tension (140 mN/m) to expand the pore left behind in the bilayer using Berendsen pressure coupling with a 2 ps coupling constant every 10 steps. The principal axis of P-gp was aligned normal to the bilayer for insertion into the pore. Lipids lining the pore were observed to collapse onto the protein surface within 750 ps of simulation at constant zero tension [72]. To maintain headgroup positions during opening and closing of the pore, phosphate sites were restrained in the z-dimension (k_z = 1000 kJ mol^{-1} nm^{-2}).

The resulting P-gp system was first equilibrated for 50 ns with the protein backbone fixed. A production run of 0.5 μs was then performed with free translational motion of the protein and a stabilizing homogeneous elastic network applied for the backbone starting crystal structure. A total of 11,365 virtual harmonic bonds (k = 150 kJ mol^{-1} nm^{-2}) were applied to Cα carbon pairs separated by two or more bonds that fell within a 10.5 Å cutoff distance in the crystal structure. Choosing this weak spring constant but large cutoff was previously shown to stabilize helical bundle and beta sheet domains while allowing the closing transition between two symmetric transmembrane (TM) domains in P-gp homolog, MsbA, via a flexible hinge region [20]. CgProt lipid bonded and nonbonded parameters were employed as reported previously [55]. The cholesterol bonded terms were adapted from Daily et al. with a harmonic force constant of 100,000 kJ mol^{-1} nm^{-2} [73].

3. Results and Discussion

3.1. Peptide insertion simulations

Independent simulations were performed for the designed helical peptides LS3, WALP27, and L24. The first batch of five simulations started with each peptide displaced 10 nm into the aqueous phase, while the second batch of five simulations for LS3 and WALP/L24 started from interfacial and transmembrane conformations, respectively. The mean length of the simulated LS3 peptide from the Cα of residue 1 to that of residue 21 was 29.5 ± 0.3 Å. This is in good agreement with the 30 Å length observed in atomistic MD [74], confirming that an ideal α-helix was maintained by the angle and dihedral restraints. The LS3 interfacial conformation exhibited an average tilt angle of 74.0° relative to the bilayer normal, consistent with the N-terminus penetrating further into the bilayer than the C-terminus (Figure 2). The helix center exhibits a mean displacement of 11.6 Å along the bilayer normal (Table 1), placing it near the carbonyl region of the bilayer centered at 1.5 nm. LS3 rotates about the helical axis so that polar sidechains point away from the nonpolar bilayer interior.

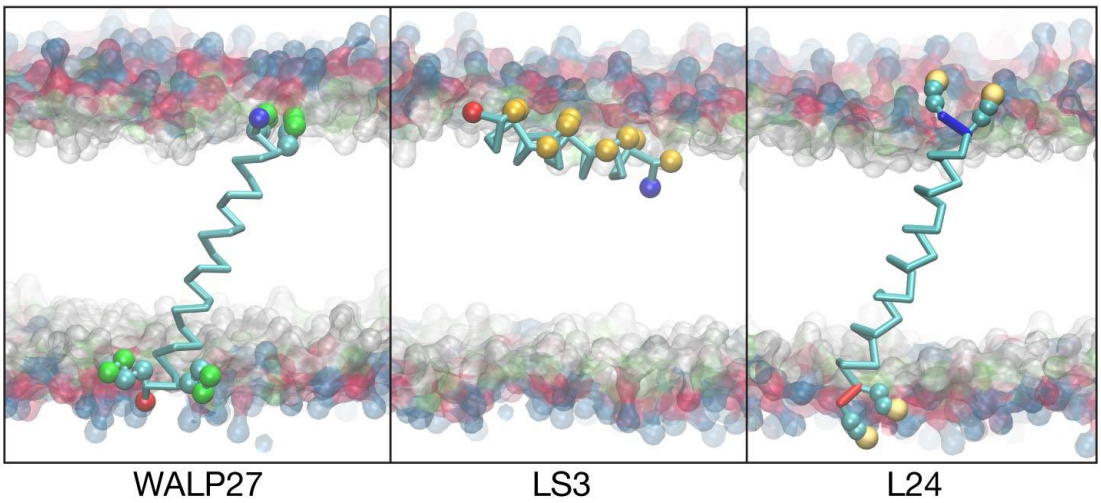

Figure 2. Equilibrated conformations in membrane-bound peptide simulations. A stable transmembrane orientation was observed in WALP and L24 simulations. LS3 simulations starting from the interfacial state persist in that conformation for at least 100 ns. The surface of lipid head groups is shown in transparent blue (choline), red (phosphate), green (glycerol) and white (esters). The Cα backbone is traced in cyan with N- and C-termini labeled blue and red, respectively. Spheres denote polar or charged sidechain sites belonging to tryptophan (green), serine (gold) and lysine (cream).

For the LS3 simulations starting from the aqueous phase, the C-terminus adsorbs to the bilayer surface as early as 1.5 ns (Figure 3). By 3 ns, the N-terminus also adsorbs onto the bilayer. The resulting interfacial state resembles the equilibrated conformation in simulations starting from the interfacial state. In all five desorbed simulations and in three out of five interfacial simulations, the N-terminus eventually crosses over to the other monolayer, with LS3 remaining in the transmembrane orientation for the remainder of the simulations (Table 2). Simulations from the interfacial state took an average of 175 ns to adopt the transmembrane configuration, while desorbed simulations took only 81 ns. These results indicate that the interfacial conformation is a metastable state. It is

noteworthy that in both the interfacial and transmembrane conformations the positive N-terminus resides at a lower depth in the bilayer than the negative C-terminus (Table 1), indicating preferential membrane interactions with the positive charge. Observing both interfacial and transmembrane orientations is consistent with previous LS3 simulations and the known ability of LS3 to oligomerize into transmembrane pores at high concentrations [66,74,69].

Table 1. Equilibrated helix orientation in DOPC simulations.

Peptide	Starting state	Helix tilt[a]	z_{center}[b] (Å)	$z_{N\text{-}term}$[c] (Å)	$z_{C\text{-}term}$[c] (Å)
LS3	interfacial	74.0 ± 8.0	11.6 ± 1.6	7.6 ± 3.0	16.8 ± 2.0
LS3	desorbed	16.3 ± 7.0	1.8 ± 1.6	11.9 ± 1.7	16.6 ±1.6
WALP	desorbed	21.2 ± 7.7	0.6 ± 1.5	16.7 ± 1.7	19.3 ± 1.6
WALP	transmembrane	22.6 ± 8.1	0.9 ± 1.5	16.2 ± 1.8	19.5 ± 1.6
L24	desorbed	82.3 ± 4.3	13.7 ± 1.6	13.4 ± 1.7	16.1 ± 2.2
L24	transmembrane	33.9 ± 5.5	0.9 ± 1.4	15.8 ± 1.7	19.2 ± 1.6

[a]Mean angle ± standard deviation of helix axis with respect to bilayer normal. [b]Mean displacement of helix center of mass from bilayer center. [c]Mean distance of terminal Cα from bilayer center.

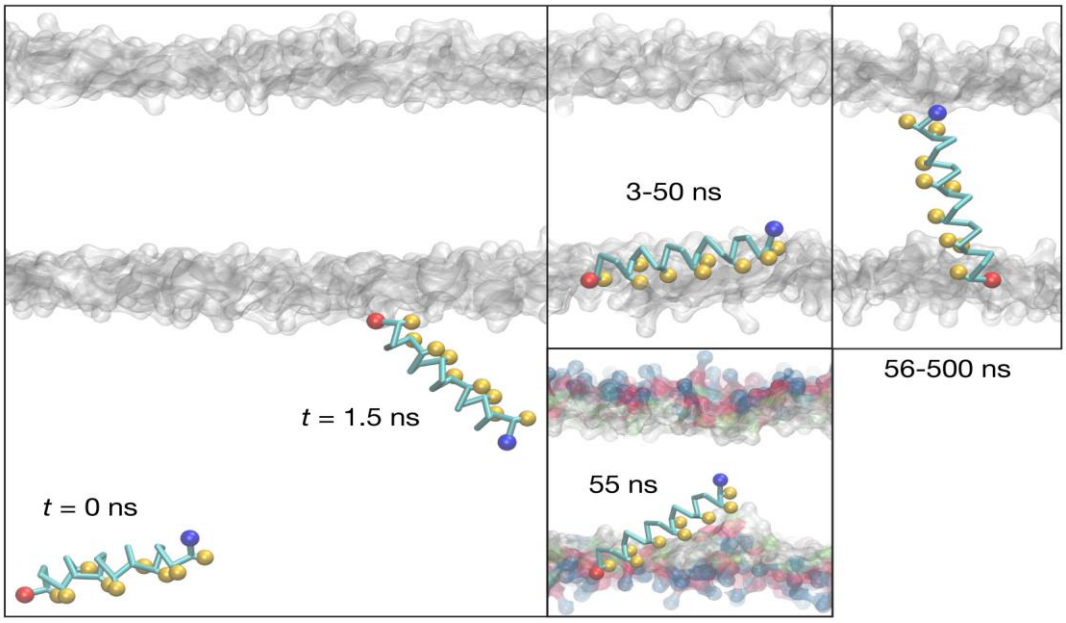

Figure 3. Sequence of events in LS3 helix insertion. The C-terminus adsorbs to the membrane surface first or at the same time as the N-terminus. The interfacial conformation lasts up to 50 ns or longer. Transient snorkeling of the phosphate head groups allows the N-terminus to spontaneously cross the bilayer.

The fact that the peptide termini are charged helps explain why the transmembrane orientation of LS3 remains anchored throughout the second simulation. A PMF was previously calculated for the insertion of uncharged LS3 peptide in DPPC using the Bond force field [66]. The simulation with neutral termini obtained a 4:1 ratio of interfacial: transmembrane helix. The interfacial conformation had an 80−90° tilt angle and 15−18 Å helix displacement, while the transmembrane conformer had a tilt of 5−20° and 0−2 Å helix displacement. These states correspond well with the two conformers predicted by CgProt, though the transmembrane state is more stabilized in the present model.

Table 2. Observed times of transmembrane insertion events in 30 independent simulation runs.

Peptide	Starting state	Insertion times (ns)	Peptide	Starting state	Insertion times (ns)
LS3	interfacial	N/A*, 176, N/A*, 105, 244	L24	transmembrane	N/A*, *, *, *, *
LS3	desorbed	56, 8, 128, 164, 50	L24	desorbed	N/A*, *, *, *, *
WALP27	desorbed	14, 21, 43, 15, 17	WALP27	transmembrane	N/A*, *, *, *, *

*Simulation run remained in its starting conformation (interfacial or transmembrane).

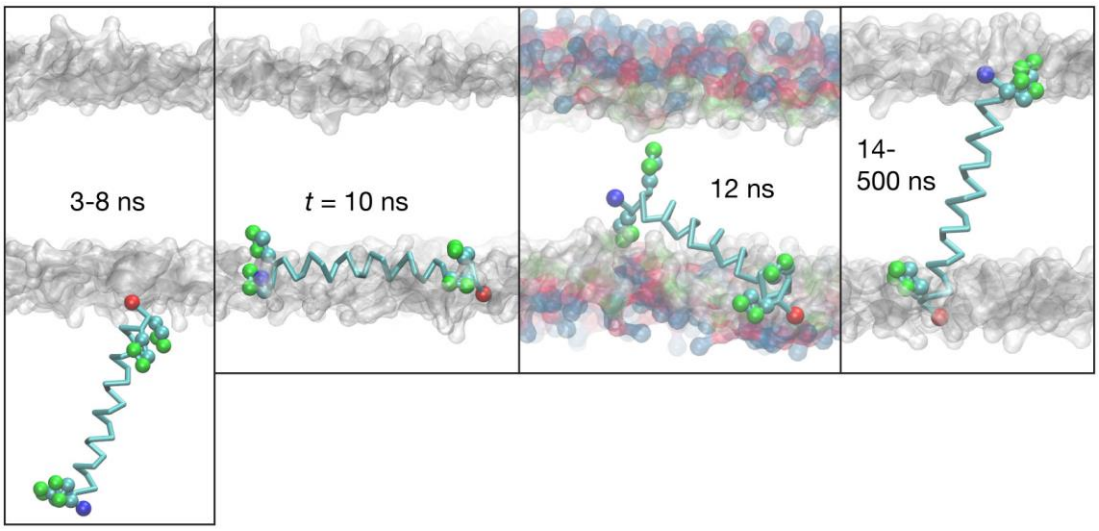

Figure 4. WALP27 helix inserts in a highly stable transmembrane conformation. The insertion of its N-terminus (blue sphere) is mediated by tryptophan interactions with glycerol and ester groups (transparent green and gray, respectively).

In contrast to LS3, only the transmembrane conformation of WALP27 is stable in the desorbed and inserted simulations. Starting from the aqueous phase, the C-terminus first docks onto the bilayer surface as early as t = 3 ns (Figure 4). The N-terminus follows suit as early as 10 ns, but the interfacial orientation with the peptide aligned with the head group bilayer region is not stable. The N-terminus continually decreases its distance to the bilayer center. As early as 12 ns, Trp 2 forms a bridge to glycerol and ester lipid sites in the other monolayer. The N-terminus then fully crosses over to the other head group region in an average of 22 ns. The resulting stable conformation is indistinguishable from the transmembrane orientation observed in simulations started from the fully inserted state.

Transmembrane WALP maintains a 22° tilt angle with its helix center <1 Å from the bilayer center. The C-terminus is found in the head group region of the bilayer near the positions of the phosphates (Table 1), while the N-terminus sits lower in the ester region that spans 1 to 2 nm from the bilayer center, again indicating enhanced permeability of the positive N-terminus. The observed degree of tilt is in agreement with the 24° ± 5° angle found by a recent fluorescence spectroscopy study of WALP23, which was intended to address discrepancies between atomistic MD simulations and previous NMR experiments [75,76]. In comparison to the transmembrane stability in CgProt, the insertion of neutral WALP in the transmembrane orientation has been observed with 80%, 100%, and 100% frequency using the MARTINI, PLUM, and GROMOS force fields, respectively [31,66].

A membrane insertion event was not observed during the desorbed simulations of the highly charged L24 peptide. Like LS3 and WALP, the C-terminus of L24 is first to adsorb to the bilayer

surface. The N-terminus soon associates with the head group region of the bilayer and adopts a lower position than the C-terminus (Table 1). The interfacial conformation of L24 was then stable throughout the remainder of the simulations, exhibiting a mean tilt angle of 82° and z-displacement of 14 Å. During the simulations starting from the transmembrane state, L24 remains anchored in a highly stable transmembrane orientation (Figure 2). The transmembrane helix exhibits a mean tilt angle of 34° and z-displacement of <1 Å. The relative positions of the N- and C-termini in transmembrane L24 are similar to the values observed for WALP, despite the two charged lysines at either end. Despite the leucine stretch of L24 being more hydrophobic than the Leu-Ala repeat in WALP, the terminal lysines apparently provide a considerable kinetic barrier to bilayer permeation. Taken together, these simulations reveal the utility and limitations of unbiased CG MD for investigating the membrane insertion of small peptides.

3.2. P-glycoprotein conformational transition

The 4M1M crystal structure (Figure 5) adopts an inward-facing conformation in which the two cytosolic nucleotide-binding domains (NBDs) belonging to its pseudo-symmetric halves are not contacting [70]. Binding of the two NBDs is required for hydrolysis of two ATP molecules at symmetrically opposed sites and subsequent substrate translocation as driven by the outward-facing conformational transition of the TM domains. In the course of the elastic network simulation, the 12 TM helices lining the accessible substrate binding chamber did not significantly change their relative orientations (3.1 Å final Cα RMSD), but motion about each TM-NBD hinge allowed the NBDs to bind each other. There was negligible intra-domain motion in each NBD (1.6 ± 0.1 Å mean RMSD).

A measure of structural openness between the NBDs is taken as the Cα distance between residues N607 and T1252 in P-gp (T561 in dimeric homolog MsbA). A range of distances is observed in crystallography and electron microscopy in the absence of substrate, suggesting flexibility in the inward-facing state [77]. In the CgProt simulation, the NBD-NBD distance rapidly decreases from 52 Å in the starting crystal structure to a final contacting distance of 30 Å. Analogously, MsbA has been crystallized in an inward-facing state in which the NBDs are partially contacting and an outward-facing ATP-bound state in which the NBD-NBD interface is fully formed. The NBDs are separated in these “closed-apo” and “nucleotide-bound” states by 37 and 35 Å, respectively [78]. The final conformation observed in the CG simulation resembles a pre-hydrolysis intermediate in which the NBD-NBD interface is fully formed and competent for ATP binding, but the opening between the TM domains still faces inward.

A homology model for P-gp was recently constructed based on the outward-facing crystal structure of Sav1866 and subjected to refinement in atomistic MD simulations [79]. One simulation in which the two MgATPs remained tightly bound resulted in an NBD separation of 37 Å (Table 3). In other simulation runs one or both of the ATPs became loosely bound, increasing the NBD separation to 39 and 41 Å, respectively. Runs performed in the absence of ATP had an NBD distance of up to 46 Å. The equilibrated conformation from the CgProt simulation resembles the “loose-tight occluded” conformation generated by atomistic MD. Each ATP binding site is formed by a Walker A motif on one NBD and an LSGGQ motif on the other NBD. Pan and Aller identified a tight ATP(O_γ) binding interaction by a 9.4 Å Cα distance between S528 and K1072 (site 2) and a loose ATP(O_α) site 1 interaction characterized by a 11-12 Å separation between the symmetrically equivalent residues K429 and S1173. The mean Walker A-LSGGQ distances in the CG simulation were 9.4 ± 0.6 Å and 17.6 ± 1.7 Å, respectively, with an even larger opening observed for site 1 (Figure 5). The

equilibrated CG trajectory exhibits a mean Cα RMSD from the loose-tight structure of 5.3 ± 0.3 Å for the NBD-NBD interface after alignment in its own reference frame.

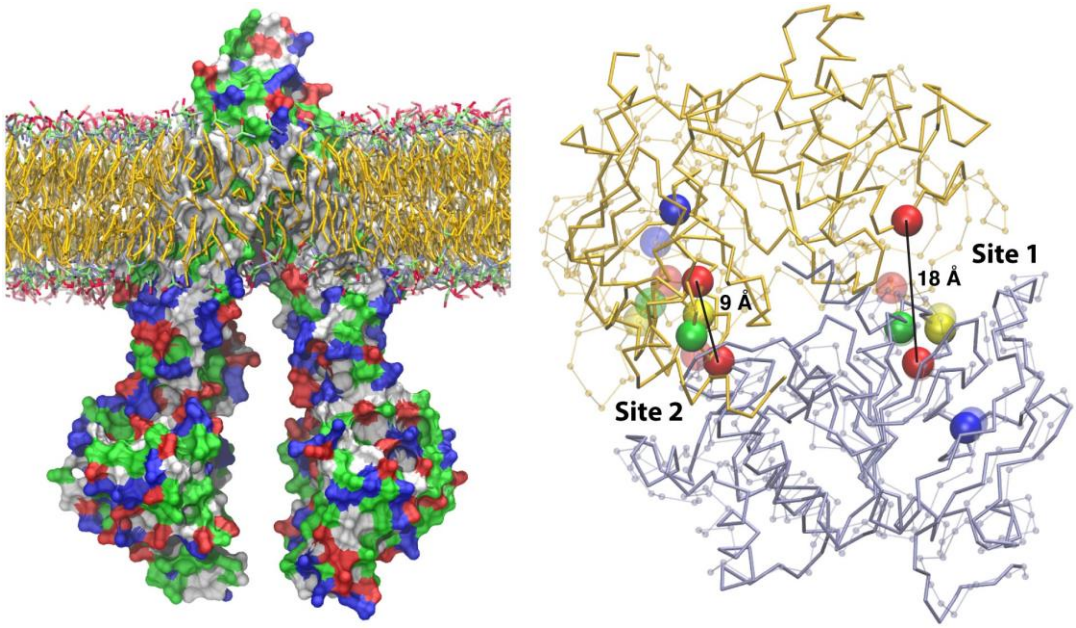

Figure 5. Left: The starting crystal structure of inward-facing P-gp (4M1M) is colored by residue polarity (gray: hydrophobic, green: hydrophilic, blue: basic, red: acidic). Right: A closing transition is observed for the cytosolic N- and C-terminal nucleotide-binding domains (steel blue and gold traces, respectively). The final snapshot is similar to the loose-tight ATP-bound conformation (transparent ball-and-stick) identified by atomistic MD [79]. The structures are aligned by superposition of NBD 1. Residues span ATP binding sites 1 and 2 (red spheres), while cross-link residues in each NBD are C427 and C1070 (yellow spheres), L435 and L1078 (blue spheres), and G423 and G1066 (green).

Several residues have been shown to participate in cysteine crosslinking across the NBDs [80,81], but this requires an alternate alignment between the NBDs. Contacts between the identified residues are only formed in the closed-apo crystal structure for MsbA, in which the NBDs are partly contacting but out of register [78]. Ward et al. posited that the closed-apo state is stabilized by bound substrate and precedes ATP binding. This would explain why ATPase activity is dramatically enhanced in the presence of substrate. The CgProt simulation adopts the fully formed NBD-NBD interface with large distances between the cross-link residues (Table 3). This is notable because the backbone potential incorporated an elastic network encoding only the open conformation. The network of contacts in the open structure thus appears predisposed for formation of the nucleotide-bound state but not the closed-apo state. In order to sample the closed-apo intermediate, an elastic network could be developed from the MsbA crystal structure based on a sequence or structural alignment with P-gp. To model transitions between the conformations, two structural states can be encoded simultaneously by the implementation of inverted Gaussian potentials in place of the unbreakable harmonic springs [11]. Changes in secondary structure have yet to be observed in elastic network simulations, but may be possible with attractive but dissociable Gaussian potentials.

Table 3. Cα distances (Å) between NBDs and crosslink residues.

MsbA residues:	T561-T561	380-380	380-388	380-376
P-gp residues:	N607-T1252	C427-C1070	C427-L435	C1070-G423
Open P-gp crystal structures[a]	46−72			
MsbA closed-apo (3B5X)[b]	37	8	19	14
MsbA nucleotide-bound (3B60)[b]	35	33	36	32
P-gp CgProt MD	30	28	34	29
Homology model[c]	37	34	36	31
Double-tight occluded[c]	37	34	36	32
Double loose[c]	41	35	39	32
Loose-tight occluded[c]	39	35	39	33
Apo run 1 (atomistic)[c]	46	39	42	35
Apo run 2 (atomistic)[c]	46	43	45	39
Apo run 3 (atomistic)[c]	39	34	39	34

[a]PDB IDs 4M2T, 4M1M, 4KSB, and 4F4C; [b]Ward et al. 2007; [c]Pan and Aller, 2015 [77-79].

3.3. Annular lipids

The P-gp simulation was performed in a physiologically representative 2 POPC: 2 POPE: cholesterol mixture to examine the role of interactions with the membrane environment. Previous simulations of MsbA in a model DOPC: DOPE bilayer revealed a solvation shell of non-specifically bound lipids bound in the grooves between TM helices [20]. With association energies of at most 1 kcal/mol and residence times below 100 ns, lipid tails were observe to dissociate from the protein and then be replaced by other lipids that adopted similar conformations on the surface of the protein, consistent with measurements on spin-labeled phospholipids [82]. To examine whether lipids preferentially associate with P-gp, the time-averaged lipid density was determined in the reference frame of the freely diffusing protein.

While POPC, POPE and cholesterol molecules do not segregate within the bulk membrane environment [55], sequestration was observed in the annulus of lipids that remained around P-gp (Figure 6) [84]. The cholesterol and phosphatidyl choline density is enriched relative to the bulk in the immediate vicinity of the protein, while no phosphatidyl ethanolamine molecules are found in the first solvation shell. A few phospholipids were also observed to diffuse into the large transmembrane chamber between the N- and C-terminal TM domains. The passage of amphiphilic lipids through the opening between the N- and C-terminal domains could potentially either mediate or compete with the uptake of xenobiotic substrates or drugs, which have been shown to have multiple distinct binding sites within the transmembrane chamber [85]. Interestingly, the smaller cholesterol molecules were not observed to enter the pore.

The lipid densities indicate that POPC and cholesterol have a slightly enhanced affinity for the exterior protein surface. Additional simulations would be needed to test whether there are any synergistic effects between the two lipids. An annular ring of loosely associated cholesterols could facilitate strong specific binding events as required for function [86] by enhancing the local sterol concentration. The preference of phosphatidyl choline for the protein was not found to be driven by

direct interactions with charged sidechains. P-gp exposes predominantly basic residues to the head group region of the inner leaflet, and choline and ethanolamine experience a similar repulsive term for positive groups in the model. The bare ethanolamine does experience a stronger attraction for acidic sidechains in the model compared to choline's methylated amine, but POPE was not found in the vicinity of the several acidic sidechains exposed to the outer leaflet. Clusters of phospholipid density in the vicinity of MsbA were previously found where the protein radius decreases near the upper portion of the inward-facing conformation [20]. We conjecture that irregularly shaped proteins create voids in the bilayer that are better filled by the bulkier PC head groups, which have weaker interactions with phosphate than PE [87].

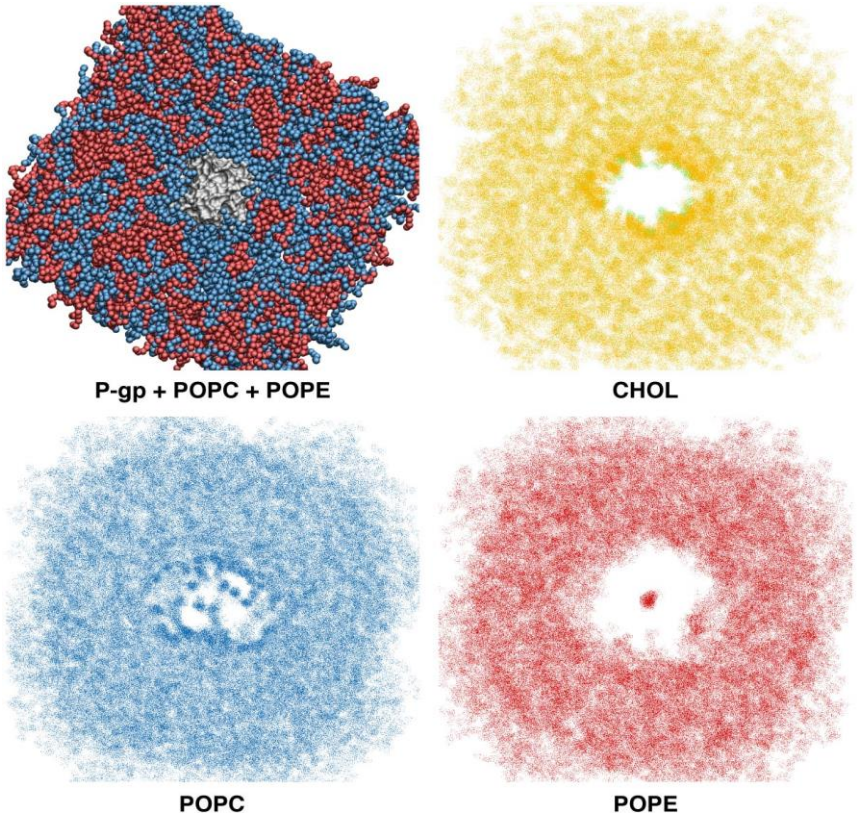

Figure 6. Top-down view of 17 nm P-gp membrane simulation. The final configuration of P-gp is drawn as gray molecular surface in the first panel using a 2.3 probe radius with cholesterol molecules omitted for clarity. The time-averaged density of each lipid in the reference frame of the protein was rendered by overlaying successive 24-ns snapshots using the solvent-cross drawing method in VMD [83]. Cholesterol −OH group density is colored green. The same perspective is used for all panels. Because periodic boundary conditions are not compatible with rotations, protein center of mass motion was removed from the trajectory by first performing a translational fit with all atoms put back inside the box, followed by a rotational fit.

4. Conclusion

CgProt enables the rapid and favorable membrane insertion of small peptides that bear minimal charge. All observed insertion events involved the N-terminus crossing the bilayer. Multiple lines of

evidence point to the attractive nature of positive-charged peptide moieties for the interface of zwitterionic membranes [88-90]. PMFs for sidechain insertion in DOPC, for example, suggest that protonated arginine and lysine are strongly attracted to the carbonyl region of the bilayer and experience a lower permeation barrier, compared to the strong repulsion experienced by deprotonated glutamate and aspartate [91]. The attraction may in part be due to water defects that have been identified in atomistic simulations, which involve the snorkeling of polar head groups to accommodate the buried charge. A similar interaction is observed in CgProt to mediate the crossing of the N-terminus of WALP between monolayers. Our observations that the free N-terminus sits deeper in the membrane than the C-terminus for three different peptides is supported by double electron-electron resonance measurements of WALP23's position in a 7:3 DPPC:PG bilayer [92].

Elastic network simulations of the P-gp open to closed conformational transition in conjunction with the CgProt force field lend support to the loose-tight structural model of ATP binding recently generated by homology modeling and atomistic MD simulation. The structural model of Pan and Aller contains an outward-facing arrangement of the TM domains, which though extensively characterized for bacterial protein MsbA, has remained elusive in experiments of the mammalian transporter P-gp. Future conformational studies with CgProt will explore the use of dissociable Gaussian potentials for modeling more subtle changes in supersecondary or tertiary structure.

In addition to driving the insertion of transmembrane helices, lipid-protein interactions are implicated in regulating the function of transmembrane proteins. Distinct from high affinity lipid binding at specific protein sites [93], molecular dynamics with CgProt reveal that the large hydrophobic TM region of P-gp and the conformational changes therein alter the local structure and diffusion of the surrounding annular lipids [20,84]. Altogether, these molecular dynamics simulations of LS3, WALP, L24, and P-gp illustrate the potentially important structural and functional roles of lipid-protein interactions and demonstrate the necessity of conducting dynamics simulations of proteins in the context of their native membrane environment.

Acknowledgments

This work was supported by National Science Foundation grant MCB-1516826 (to R.D.H.). Cody Black was supported by an American Foundation for Pharmaceutical Education Gateway to Research Award.

Conflict of Interest

The authors declare no conflicts of interest in this paper.

References

1. Barrera NP, Zhou M, Robinson CV (2013) The role of lipids in defining membrane protein interactions: Insights from mass spectrometry. *Trends Cell Biol* 23: 1-8.
2. Smith AW (2012) Lipid-protein interactions in biological membranes: A dynamic perspective. *Biochim Biophys Acta Biomembr* 1818: 172-177.
3. Martinez-Seara H, Rog T, Karttunen M, et al. (2008) Influence of cis double-bond parametrization on lipid membrane properties: How seemingly insignificant details in force-field change even qualitative trends. *J Chem Phys* 129: 105103.

4. Ogata K, Nakamura S (2015) Improvement of parameters of the AMBER potential force field for phospholipids for description of thermal phase transitions. *J Phys Chem B* 119: 9726-9739.
5. Venable RM, Brown FL, Pastor RW (2015) Mechanical properties of lipid bilayers from molecular dynamics simulation. *Chem Phys Lipids* 192: 60-74.
6. Paloncyova M, Fabre G, DeVane RH, et al. (2014) Benchmarking of force fields for molecule-membrane interactions. *J Chem Theory Comput* 10: 4143-4151.
7. Venable RM, Ingolfsson HI, Lerner MG, et al. (2017) Lipid and peptide diffusion in bilayers: The Saffman-Delbruck model and periodic boundary conditions. *J Phys Chem B* 121: 3443-3457.
8. Perilla JR, Goh BC, Cassidy CK, et al. (2015) Molecular dynamics simulations of large macromolecular complexes. *Curr Opin Struct Biol* 31: 64-74.
9. Baaden M, Marrink SJ (2013) Coarse-grain modelling of protein-protein interactions. *Curr Opin Struct Biol* 23: 878-886.
10. Hills Jr RD, Brooks III CL (2009) Insights from coarse-grained Go models for protein folding and dynamics. *Int J Mol Sci* 10: 889-905.
11. Hills Jr RD (2014) Balancing bond, nonbond, and Go-like terms in coarse grain simulations of conformational dynamics. *Methods Mol Biol* 1084: 123-140.
12. Jackson J, Nguyen K, Whitford PC (2015) Exploring the balance between folding and functional dynamics in proteins and RNA. *Int J Mol Sci* 16: 6868-6889.
13. Kmiecik S, Gront D, Kolinski M, et al. (2016) Coarse-grained protein models and their applications. *Chem Rev* 116: 7898-7936.
14. Ramirez CL, Petruk A, Bringas M, et al. (2016) Coarse-grained simulations of heme proteins: Validation and study of large conformational transitions. *J Chem Theory Comput* 12: 3390-3397.
15. De Sancho D, Best RB (2012) Modulation of an IDP binding mechanism and rates by helix propensity and non-native interactions: Association of HIF1alpha with CBP. *Mol Biosyst* 8: 256-267.
16. Periole X, Cavalli M, Marrink SJ, et al. (2009) Combining an elastic network with a coarse-grained molecular force field: Structure, dynamics, and intermolecular recognition. *J Chem Theory Comput* 5: 2531-2543.
17. Shen H, Moustafa IM, Cameron CE, et al. (2012) Exploring the dynamics of four RNA-dependent RNA polymerases by a coarse-grained model. *J Phys Chem B* 116: 14515-14524.
18. Dony N, Crowet JM, Joris B, et al. (2013) SAHBNET, an accessible surface-based elastic network: An application to membrane protein. *Int J Mol Sci* 14: 11510-11526.
19. Shimamura T, Weyand S, Beckstein O, et al. (2010) Molecular basis of alternating access membrane transport by the sodium-hydantoin transporter Mhp1. *Science* 328: 470-473.
20. Ward AB, Guvench O, Hills Jr RD (2012) Coarse grain lipid-protein molecular interactions and diffusion with MsbA flippase. *Proteins* 80: 2178-2190.
21. Prasanna X, Sengupta D, Chattopadhyay A (2016) Cholesterol-dependent conformational plasticity in GPCR dimers. *Sci Rep* 6: 31858.
22. Poyry S, Vattulainen I (2016) Role of charged lipids in membrane structures: Insight given by simulations. *Biochim Biophys Acta Biomembr* 1858: 2322-2333.
23. Hedger G, Sansom MS (2016) Lipid interaction sites on channels, transporters and receptors: Recent insights from molecular dynamics simulations. *Biochim Biophys Acta Biomembr* 1858: 2390-2400.

24. Provasi D, Boz MB, Johnston JM, et al. (2015) Preferred supramolecular organization and dimer interfaces of opioid receptors from simulated self-association. *PLOS Comput Biol* 11: e1004148.
25. Kalli AC, Sansom MS, Reithmeier RA (2015) Molecular dynamics simulations of the bacterial UraA H^+-uracil symporter in lipid bilayers reveal a closed state and a selective interaction with cardiolipin. *PLOS Comput Biol* 11: e1004123.
26. Marrink SJ, Risselada HJ, Yefimov S, et al. (2007) The MARTINI force field: Coarse grained model for biomolecular simulations. *J Phys Chem B* 111: 7812-7824.
27. de Jong DH, Periole X, Marrink SJ (2012) Dimerization of amino acid side chains: Lessons from the comparison of different force fields. *J Chem Theory Comput* 8: 1003-1014.
28. Singh G, Tieleman DP (2011) Using the Wimley-White hydrophobicity scale as a direct quantitative test of force fields: The MARTINI coarse-grained model. *J Chem Theory Comput* 7: 2316-2324.
29. Stark AC, Andrews CT, Elcock AH (2013) Toward optimized potential functions for protein-protein interactions in aqueous solutions: Osmotic second virial coefficient calculations using the MARTINI coarse-grained force field. *J Chem Theory Comput* 9: 4176-4185.
30. Bereau T, Kremer K (2016) Protein-backbone thermodynamics across the membrane interface. *J Phys Chem B* 120: 6391-6400.
31. Bereau T, Bennett WF, Pfaendtner J, et al. (2015) Folding and insertion thermodynamics of the transmembrane WALP peptide. *J Chem Phys* 143: 243127.
32. Rodgers JM, Sorensen J, de Meyer FJ, et al. (2012) Understanding the phase behavior of coarse-grained model lipid bilayers through computational calorimetry. *J Phys Chem B* 116: 1551-1569.
33. Arnarez C, Uusitalo JJ, Masman MF, et al. (2015) Dry Martini, a coarse-grained force field for lipid membrane simulations with implicit solvent. *J Chem Theory Comput* 11: 260-275.
34. Ingolfsson HI, Melo MN, van Eerden FJ, et al. (2014) Lipid organization of the plasma membrane. *J Am Chem Soc* 136: 14554-14559.
35. Melo MN, Ingolfsson HI, Marrink SJ (2015) Parameters for Martini sterols and hopanoids based on a virtual-site description. *J Chem Phys* 143: 243152.
36. Paloncyova M, Vavrova K, Sovova Z, et al. (2015) Structural changes in ceramide bilayers rationalize increased permeation through stratum corneum models with shorter acyl tails. *J Phys Chem B* 119: 9811-9819.
37. Periole X, Marrink SJ (2013) The Martini coarse-grained force field. *Methods Mol Biol* 924: 533-565.
38. Marrink SJ, Tieleman DP (2013) Perspective on the Martini model. *Chem Soc Rev* 42: 6801-6822.
39. Baron R, de Vries AH, Hunenberger PH, et al. (2006) Comparison of atomic-level and coarse-grained models for liquid hydrocarbons from molecular dynamics configurational entropy estimates. *J Phys Chem B* 110: 8464-8473.
40. Hills Jr RD, Lu L, Voth GA (2010) Multiscale coarse-graining of the protein energy landscape. *PLOS Comput Biol* 6: e1000827.
41. Jia Z, Chen J (2016) Necessity of high-resolution for coarse-grained modeling of flexible proteins. *J Comput Chem* 37: 1725-1733.
42. Miguel V, Perillo MA, Villarreal MA (2016) Improved prediction of bilayer and monolayer properties using a refined BMW-MARTINI force field. *Biochim Biophys Acta Biomembr* 1858: 2903-2910.

43. Wu Z, Cui Q, Yethiraj A (2010) A new coarse-grained model for water: The importance of electrostatic interactions. *J Phys Chem B* 114: 10524-10529.
44. Wu Z, Cui Q, Yethiraj A (2011) A new coarse-grained force field for membrane-peptide simulations. *J Chem Theory Comput* 7: 3793-3802.
45. Yesylevskyy SO, Schafer LV, Sengupta D, et al. (2010) Polarizable water model for the coarse-grained MARTINI force field. *PLOS Comput Biol* 6: e1000810.
46. de Jong DH, Singh G, Bennett WFD, et al. (2013) Improved parameters for the Martini coarse-grained protein force field. *J Chem Theory Comput* 9: 687-697.
47. Lu L, Voth GA (2009) Systematic coarse-graining of a multicomponent lipid bilayer. *J Phys Chem B* 113: 1501-1510.
48. Wang ZJ, Deserno M (2010) A systematically coarse-grained solvent-free model for quantitative phospholipid bilayer simulations. *J Phys Chem B* 114: 11207-11220.
49. Han W, Schulten K (2012) Further optimization of a hybrid united-atom and coarse-grained force field for folding simulations: Improved backbone hydration and interactions between charged side chains. *J Chem Theory Comput* 8: 4413-4424.
50. Han W, Wan CK, Wu YD (2008) Toward a coarse-grained protein model coupled with a coarse-grained solvent model: Solvation free energies of amino acid side chains. *J Chem Theory Comput* 4: 1891-1901.
51. Ganesan SJ, Matysiak S (2014) Role of backbone dipole interactions in the formation of secondary and supersecondary structures of proteins. *J Chem Theory Comput* 10: 2569-2576.
52. Noid WG, Chu JW, Ayton GS, et al. (2008) The multiscale coarse-graining method. I. A rigorous bridge between atomistic and coarse-grained models. *J Chem Phys* 128: 244114.
53. Noid WG, Chu JW, Ayton GS, et al. (2007) Multiscale coarse-graining and structural correlations: Connections to liquid-state theory. *J Phys Chem B* 111: 4116-4127.
54. Pall S, Abraham MJ, Kutzner C, et al. (2015) Tackling exascale software challenges in molecular dynamics simulations with GROMACS. *Proc EASC 2015 LNCS* 8759: 3-27.
55. Hills Jr RD, McGlinchey N (2016) Model parameters for simulation of physiological lipids. *J Comput Chem* 37: 1112-1118.
56. Monticelli L, Kandasamy SK, Periole X, et al. (2008) The MARTINI coarse-grained force field: Extension to proteins. *J Chem Theory Comput* 4: 819-834.
57. Bond PJ, Wee CL, Sansom MS (2008) Coarse-grained molecular dynamics simulations of the energetics of helix insertion into a lipid bilayer. *Biochemistry* 47: 11321-11331.
58. Winger M, Trzesniak D, Baron R, et al. (2009) On using a too large integration time step in molecular dynamics simulations of coarse-grained molecular models. *Phys Chem Chem Phys* 11: 1934-1941.
59. Karanicolas J, Brooks III CL (2002) The origins of asymmetry in the folding transition states of protein L and protein G. *Protein Sci* 11: 2351-2361.
60. Bereau T, Deserno M (2009) Generic coarse-grained model for protein folding and aggregation. *J Chem Phys* 130: 235106.
61. Herzog FA, Braun L, Schoen I, et al. (2016) Improved side chain dynamics in MARTINI simulations of protein-lipid interfaces. *J Chem Theory Comput* 12: 2446-24458.
62. Cerutti DS, Duke R, Freddolino PL, et al. (2008) Vulnerability in popular molecular dynamics packages concerning Langevin and Andersen dynamics. *J Chem Theory Comput* 4: 1669-1680.

63. Bereau T, Wang ZJ, Deserno M (2014) More than the sum of its parts: Coarse-grained peptide-lipid interactions from a simple cross-parametrization. *J Chem Phys* 140: 115101.
64. Bond PJ, Holyoake J, Ivetac A, et al. (2007) Coarse-grained molecular dynamics simulations of membrane proteins and peptides. *J Struct Biol* 157: 593-605.
65. Kar P, Gopal SM, Cheng YM, et al. (2014) Transferring the PRIMO coarse-grained force field to the membrane environment: Simulations of membrane proteins and helix-helix association. *J Chem Theory Comput* 10: 3459-3472.
66. Hall BA, Chetwynd AP, Sansom MS (2011) Exploring peptide-membrane interactions with coarse-grained MD simulations. *Biophys J* 100: 1940-1948.
67. Kim T, Im W (2010) Revisiting hydrophobic mismatch with free energy simulation studies of transmembrane helix tilt and rotation. *Biophys J* 99: 175-183.
68. Liu F, Lewis RN, Hodges RS, et al. (2004) Effect of variations in the structure of a polyleucine-based alpha-helical transmembrane peptide on its interaction with phosphatidylethanolamine bilayers. *Biophys J* 87: 2470-2482.
69. Lear JD, Wasserman ZR, DeGrado WF (1988) Synthetic amphiphilic peptide models for protein ion channels. *Science* 240: 1177-1181.
70. Li J, Jaimes KF, Aller SG (2014) Refined structures of mouse P-glycoprotein. *Protein Sci* 23: 34-46.
71. Costa JA, Nguyen DA, Leal-Pinto E, et al. (2013) Wicking: A rapid method for manually inserting ion channels into planar lipid bilayers. *PLOS ONE* 8: e60836.
72. Javanainen M (2014) Universal method for embedding proteins into complex lipid bilayers for molecular dynamics simulations. *J Chem Theory Comput* 10: 2577-2582.
73. Daily MD, Olsen BN, Schlesinger PH, et al. (2014) Improved coarse-grained modeling of cholesterol-containing lipid bilayers. *J Chem Theory Comput* 10: 2137-2150.
74. Nguyen TH, Liu Z, Moore PB (2013) Molecular dynamics simulations of homo-oligomeric bundles embedded within a lipid bilayer. *Biophys J* 105: 1569-1580.
75. Holt A, Koehorst RB, Rutters-Meijneke T, et al. (2009) Tilt and rotation angles of a transmembrane model peptide as studied by fluorescence spectroscopy. *Biophys J* 97: 2258-2266.
76. Ozdirekcan S, Etchebest C, Killian JA, et al. (2007) On the orientation of a designed transmembrane peptide: Toward the right tilt angle? *J Am Chem Soc* 129: 15174-15181.
77. Moeller A, Lee SC, Tao H, et al. (2015) Distinct conformational spectrum of homologous multidrug ABC transporters. *Structure* 23: 450-460.
78. Ward AB, Reyes CL, Yu J, et al. (2007) Flexibility in the ABC transporter MsbA: Alternating access with a twist. *Proc Natl Acad Sci USA* 104: 19005-19010.
79. Pan L, Aller SG (2015) Equilibrated atomic models of outward-facing P-glycoprotein and effect of ATP binding on structural dynamics. *Sci Rep* 5: 7880.
80. Loo TW, Clarke DM (2000) Drug-stimulated ATPase activity of human P-glycoprotein is blocked by disulfide cross-linking between the nucleotide-binding sites. *J Biol Chem* 275: 19435-19438.
81. Urbatsch IL, Gimi K, Wilke-Mounts S, et al. (2001) Cysteines 431 and 1074 are responsible for inhibitory disulfide cross-linking between the two nucleotide-binding sites in human P-glycoprotein. *J Biol Chem* 276: 26980-26987.
82. East JM, Melville D, Lee AG (1985) Exchange rates and numbers of annular lipids for the calcium and magnesium ion dependent adenosinetriphosphatase. *Biochemistry* 24: 2615-2623.

83. Humphrey W, Dalke A, Schulten K (1996) VMD: Visual molecular dynamics. *J Mol Graph* 14: 33-38.
84. Bechara C, Noll A, Morgner N, et al. (2015) A subset of annular lipids is linked to the flippase activity of an ABC transporter. *Nat Chem* 7: 255-262.
85. Aller SG, Yu J, Ward AB, et al. (2009) Structure of P-glycoprotein reveals a molecular basis for poly-specific drug binding. *Science* 323: 1718-1722.
86. Habeck M, Haviv H, Katz A, et al. (2015) Stimulation, inhibition, or stabilization of Na,K-ATPase caused by specific lipid interactions at distinct sites. *J Biol Chem* 290: 4829-4842.
87. Kucerka N, van Oosten B, Pan J, et al. (2015) Molecular structures of fluid phosphatidylethanolamine bilayers obtained from simulation-to-experiment comparisons and experimental scattering density profiles. *J Phys Chem B* 119: 1947-1956.
88. Gleason NJ, Vostrikov VV, Greathouse DV, et al. (2013) Buried lysine, but not arginine, titrates and alters transmembrane helix tilt. *Proc Natl Acad Sci USA* 110: 1692-1695.
89. Hu Y, Sinha SK, Patel S (2014) Reconciling structural and thermodynamic predictions using all-atom and coarse-grain force fields: The case of charged oligo-arginine translocation into DMPC bilayers. *J Phys Chem B* 118: 11973-11992.
90. Sun D, Forsman J, Woodward CE (2015) Evaluating force fields for the computational prediction of ionized arginine and lysine side-chains partitioning into lipid bilayers and octanol. *J Chem Theory Comput* 11: 1775-1791.
91. MacCallum JL, Bennett WF, Tieleman DP (2008) Distribution of amino acids in a lipid bilayer from computer simulations. *Biophys J* 94: 3393-3404.
92. Matalon E, Kaminker I, Zimmermann H, et al. (2013) Topology of the trans-membrane peptide WALP23 in model membranes under negative mismatch conditions. *J Phys Chem B* 117: 2280-2293.
93. Clay AT, Lu P, Sharom FJ (2015) Interaction of the p-glycoprotein multidrug transporter with sterols. *Biochemistry* 54: 6586-6597.

AIMS Press